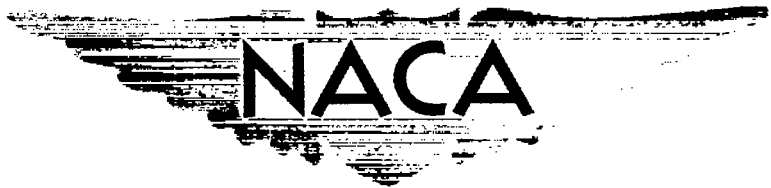


NACA RM L51L17

CLASSIFICATION CANCELLED

UNCLASSIFIED

By authority of *77ACB Rev a/b*
Effective 1/24/58
DRN-124
Am 7-12-58



RESEARCH MEMORANDUM

AN INVESTIGATION OF A SUPERSONIC AIRCRAFT CONFIGURATION
HAVING A TAPERED WING WITH CIRCULAR-ARC
SECTIONS AND 40° SWEEPBACK

ESTIMATED DOWNWASH ANGLES DERIVED FROM PRESSURE
MEASUREMENTS ON THE TAIL AT MACH
NUMBERS OF 1.40 AND 1.59

By Frederick C. Grant and John P. Gapcynski

Langley Aeronautical Laboratory
Langley Field, Va.

FOR REFERENCE

CLASSIFIED DOCUMENT

NOT TO BE TAKEN FROM THIS ROOM

This material contains information affecting the National Defense of the United States within the meaning of the espionage laws, Title 18, U.S.C., Secs. 793 and 794, the transmission or revelation of which in any manner to unauthorized person is prohibited by law.

NATIONAL ADVISORY COMMITTEE FOR AERONAUTICS

WASHINGTON

March 10, 1952



NACA LIBRARY
LANGLEY AERONAUTICAL LABORATORY
Langley Field, Va.



NATIONAL ADVISORY COMMITTEE FOR AERONAUTICS

RESEARCH MEMORANDUM

AN INVESTIGATION OF A SUPERSONIC AIRCRAFT CONFIGURATION

HAVING A TAPERED WING WITH CIRCULAR-ARC

SECTIONS AND 40° SWEEPBACK

ESTIMATED DOWNWASH ANGLES DERIVED FROM PRESSURE

MEASUREMENTS ON THE TAIL AT MACH

NUMBERS OF 1.40 AND 1.59

By Frederick C. Grant and John P. Gapcynski

SUMMARY

From an analysis of pressures measured on the horizontal tail of a supersonic aircraft configuration in the Langley 4- by 4-foot supersonic tunnel at Mach numbers of 1.40 and 1.59 estimates of downwash angle in the plane of the tail are obtained for the complete model and the model less the wing. These results are compared with an approximate application of linearized theory and, where appropriate, with force-tests results for the same configuration.

The downwash angles obtained from the pressure measurements were found to be everywhere greater than those of the theory. This appears to be due largely to the neglect of the flow field produced by the vertical tail. There was reasonable agreement in the average rate of change of downwash angle with angle of attack with the exception of those values obtained nearest the vertical tail.

Both the pressure data and the theoretical results indicate that about half of the total rate of change of downwash angle with angle of attack is due to the wing at a Mach number of 1.40. At a Mach number of 1.59, theory indicates the same trend. Experimentally at $M = 1.59$, however, pressure downwash angles show a somewhat smaller wing contribution to the rate of change of downwash angle with angle of attack, while on the other hand, force results at the same Mach number show a greater wing contribution.

INTRODUCTION

A knowledge of the downwash field at the tail of a supersonic aircraft configuration is essential to the determination of the static longitudinal stability of the aircraft. Most of the supersonic downwash field measurements have been made behind isolated wings as in references 1 to 5. References 1 to 3 contain measurements of the downwash field at $M = 1.53$ for rectangular, triangular, and swept wings, respectively. Reference 4 presents field measurements behind a rectangular wing at $M = 2.41$ and reference 5 gives values behind a trapezoidal wing at $M = 1.91$. In reference 6, over-all downwash values at the tail as derived from force-test data are given for a rectangular wing and tail and body combination at $M = 1.92$. Force-test downwash values for the 40° swept-wing and swept-tail configuration of this paper are given in reference 7 for $M = 1.40$ and reference 8 for $M = 1.59$.

Linearized solutions for the downwash fields of wings of various shapes may be found in the works of Lagerstrom and Graham (references 9 and 10) who use the method of superposition of conical flow solutions; Lomax and Sluder (reference 11) who use a surface of potential discontinuity formed by a distribution of doublets; and Mirels and Haefeli (reference 12) who use the discontinuity formed by a distribution of vortices. The method of reference 12 was used for the wing of the configuration of this paper.

The flow fields over bodies of revolution may be calculated by the method of characteristics as discussed in reference 13 for 0° angle of attack and in reference 14 for angles of attack other than 0° . Linearized theory calculations for corresponding attitudes may be made by the methods of references 15 and 16 which were used for the calculation of the body downwash fields in this paper.

The tail data used in this paper were taken in the course of the body and wing pressure tests reported in references 17 to 20. The estimated downwash angles given in this paper are supplementary results of the tests on a supersonic aircraft configuration having a 40° sweptback wing at Mach numbers of 1.40 and 1.59. By use of the pressure measurements on the horizontal tail surfaces the effective downwash angles at the tail have been approximated by determining the tail incidence angles for which the lifting pressure vanished. Results are given for the complete configuration and for the model less the wing.

The results are compared with an approximate application of linear theory calculations and with downwash angles derived from force tests (references 7 and 8) on the same configuration. The complexity of the

configuration and the approximate nature of the pressure downwash angles to which the theory is compared do not justify a more complete theoretical treatment.

SYMBOLS

Free-stream conditions:

ρ	mass density of air
V	airspeed
a	speed of sound in air
M	Mach number (V/a)
q	dynamic pressure $\left(\frac{1}{2}\rho V^2\right)$
p	static pressure

Horizontal-tail geometry:

S	area
b	span
c	chord parallel to free stream at any spanwise station
c'	chord of orifice plane normal to quarter-chord line
x	chordwise distance from airfoil leading edge
x'	chordwise distance from airfoil leading edge in plane normal to quarter-chord line
\bar{c}	average chord (S/b)
y	spanwise distance from plane of symmetry of model

Pressure data:

p_l	local static pressure
-------	-----------------------

P pressure coefficient $\left(\frac{P_L - P}{q} \right)$

ΔP lifting-pressure coefficient $(P_L - P_U)$

Downwash determination:

α angle of attack of fuselage center line (positive up), degrees

i_t tail incidence angle relative to fuselage center line
(positive up), degrees

ϵ downwash angle at tail (positive down), degrees

Δc_n average lifting-pressure coefficient on chord segment
(positive up) between 15- and 45-percent constant chord lines

$$\left(\frac{1}{0.45 - 0.15} \int_{0.15}^{0.45} \Delta P d(x/c) \text{ or } \frac{1}{0.41 - 0.13} \int_{0.13}^{0.41} \Delta P d(x'/c') \right)$$

ΔC_N average lifting-pressure coefficient on spanwise strip
(positive up) between 15- and 45-percent constant chord lines

$$\left(\frac{2}{b} \int_0^{b/2} \left(\Delta c_n \frac{c}{c} \right) dy \right)$$

Subscripts:

L lower surface

U upper surface

Tunnel.- The data presented in this paper were obtained in the Langley 4- by 4-foot supersonic tunnel at Mach numbers of 1.40 and 1.59. A detailed description of this tunnel may be found in reference 17.

Model.- The sting-mounted steel test model (fig. 1) was built to the dimensions given in figure 2. The afterpiece shown in figure 1 is integral with the model and forms a part of the sting as shown in figure 3. The detachable wing of the model had 40° of sweepback at the quarter-chord line, aspect ratio 4, taper ratio 0.5, and 10-percent-thick circular-arc sections normal to the quarter-chord line.

The horizontal tail had 40° sweepback at the quarter-chord line, aspect ratio 3.72, taper ratio 0.5, and NACA 65-008 sections normal to the quarter-chord line.

The tail incidence angles were set at the root by means of machined filler blocks which fitted around the horizontal tail and into a cut-out in the rudder. The pivot axis for the horizontal tail passed through the 73-percent point of the root chord. There were 35 orifices arranged in three vertical planes on the left half of the horizontal tail. The number and location of the orifices were limited by the thinness of the tail. The position of each orifice is given in table I, while in figure 4 are shown the positions of the orifice planes and the spanwise strip used in the analysis of the pressure data.

TESTS

Experimental data were obtained at Mach numbers of 1.40 and 1.59 and Reynolds numbers (based on the wing mean aerodynamic chord) of 600,000 and 575,000, respectively, for the complete model and the model less the wing. The angle-of-attack range of the complete model was -3° to 8° at $M = 1.40$ and -5° to 10° at $M = 1.59$. The model less the wing was tested for an angle-of-attack range of -5° to 4° at $M = 1.40$ and -5° to 10° at $M = 1.59$. The tail incidence angles for each angle of attack are shown in tables I and II. The data were obtained for stagnation conditions of: pressure, 0.25 atmosphere; temperature, 110° Fahrenheit; dew points of -30° Fahrenheit at $M = 1.40$, and -35° Fahrenheit at $M = 1.59$.

PRECISION OF TESTS AND RESULTS

Calibration data for the test section at Mach number 1.40 may be found in reference 18 and at Mach number 1.59 in reference 17. Since the gradients of flow parameters are small in the vicinity of the model, no corrections have been made to the data.

The estimated extreme variations of M and P through the test section are ± 0.01 . The estimated error in P at a given point of the test section is ± 0.003 .

The accuracy attained in setting the angles α and i_t is estimated as $\pm 0.02^\circ$ and $\pm 0.05^\circ$, respectively.

The estimated maximum error in ϵ due to the local variation of P , to the setting of α and i_t , and to changes in the fairing of the pressure distributions and the loading curves of the spanwise strip is $\pm 0.25^\circ$.

Presentation and Analysis of Experimental Data

In tables I and II, the data obtained for the horizontal tail are given in pressure-coefficient form.

In each orifice plane, point downwash angles were obtained from the data by determining the tail incidence angles for which the lifting pressure vanished at the 15-percent constant chord line. At these incidence angles, the chord line of the orifice plane was considered to be aligned with the flow at the leading edge in the orifice plane and the downwash angle was found from the relation $\epsilon = \alpha + i_t$. Curves of the variation of this point downwash angle with angle of attack are given in figure 5 for the model at $M = 1.40$ and 1.59 , with and without the wing.

The point downwash angle described is not the angle of downward deviation of the flow in the absence of the tail, which is the usual concept of a downwash angle. The fact that each point of analysis is behind a detached shock and includes a considerable length of leading edge in its fore Mach cone makes the point downwash analysis yield a value of downwash angle determined by local conditions in the fore Mach cone. In addition, the interference effects of the body-wing-rudder combination may vary the flow field at the tail. The point downwash angles derived from the pressure analysis are to be considered then as approximations to the usual point downwash angles and not identical with them. The reason the values are considered as approximations to the

downwash angle and as such compared with theory is that the horizontal tail is a comparatively large distance above the trailing-vortex sheet from the wing and the part of the tail in the fore Mach cone is subject to a comparatively uniform flow.

The area downwash angles are presented in figure 6. To find the area downwash angles, the normal-force coefficient ΔC_N on a chord segment between the 15- and 45-percent constant chord lines, was found in each orifice plane. These normal-force coefficients were plotted against the spanwise station as shown in figure 7 and were then integrated. The vanishing of this integral ΔC_N with tail incidence angle was taken to indicate an average heading of the local air stream for the strip bounded by the 15- and 45-percent constant chord lines. A sample variation of ΔC_N with tail incidence angle is shown in figure 8 along with the derived area downwash angle.

If sufficient orifices were available over the entire tail, the area downwash angles would be those corresponding to the vanishing of the tail normal-force coefficient.

THEORETICAL ANALYSIS

Theoretical calculations of the downwash field in the region of the tail of the model were made for the fuselage alone (less canopies) and the wing alone. Point downwash values were obtained at the same chordwise locations, and chordwise and spanwise integrations were performed for the same region of the tail used in the analysis of the experimental data. For the case of the wing-fuselage combination, the values of the downwash were approximated by superposition of the wing and body values.

The body downwash values were determined from linear calculations (references 15 and 16) of the flow field about the fuselage in the vicinity of the tail.

The wing downwash values were calculated by the method of reference 12. This analysis (reference 12) is based on a line vortex located at a straight-line approximation to the locus of the centers of pressure of the individual wing stations. For the present application, this straight-line approximation intersected the root chord at the 50-percent station for both Mach numbers, and the tip chord at the 35-percent station for a Mach number of 1.59, and the 10-percent station for a Mach number of 1.40.

The theoretical span loadings used to establish both the position and magnitude of the line vortex were obtained from references 19 and 20 for Mach numbers of 1.59 and 1.40, respectively.

The downwash calculations were made for a fixed-tail-plane position relative to the plane of the wing at an angle of attack of 0° . No allowance was made for either the drop in tail position as the wing angle of attack was increased, or the displacement of the trailing-vortex sheet. Actually, the vortex sheet will displace downward as the angle of attack is increased and the tail position drops so that the two effects will tend to cancel each other.

The rolling up of the trailing-vortex sheet has a negligible effect on the downwash angles for this configuration because of the location of the horizontal tail. The short-span-tail plane is not far enough downstream of the wing tips to be affected by the rolling-up process which starts at the tips (reference 21).

RESULTS AND DISCUSSION

Variation of point downwash angles with α . - In figure 5, for both the complete model and the model less the wing, the variations with angle of attack of the point-downwash angles derived from the pressure data are presented along with corresponding theoretical variations.

All the point downwash values are somewhat higher than the corresponding theory for both the complete model and the model less wing. Considering the influence of the vertical tail, which is neglected in the theory, helps to account for this difference. The velocity increase at the horizontal-tail location, caused by the vertical-tail thickness, occurs mostly normal to the leading edge and since the vertical tail has a sweptback leading edge, it tends to increase the experimental downwash angles. If average slopes are taken over the range of angles of attack for which there are data, the $ds/d\alpha$ as indicated by the point downwash-angle variations are much the same as those indicated by theory, except in the inboard plane for the model less the wing. At $M = 1.59$, (fig. 5(b)), the point downwash-angle variation for the inboard plane indicates a somewhat higher $ds/d\alpha$ than the theory.

The difference curves of figure 5 represent the downwash angle due to the addition of the wing. Although they are subject to twice the error of either of the other curves taken alone, the agreement in angle and slope is good for the two outboard stations at both Mach numbers. At the inboard station at $M = 1.59$, the large body contribution indicated by the pressure downwash leads to a negative $ds/d\alpha$ over the positive α range and the largest disagreement with theory.

Variation of downwash angle with spanwise position.- In the tail span-loading curves of figure 7, there is, for angles of attack greater than zero, an evident gradient along the span in the i_t required for zero Δc_n . If the vanishing of Δc_n is taken as the criterion for alinement of the chord of a spanwise station with the local flow, and the downwash angle computed as $\epsilon = \alpha + i_t$, an increase in downwash angle from the outboard to the inboard orifice planes is indicated. A larger gradient is shown for the model less the wing than for the complete model, indicating a large body contribution to $d\epsilon/d\alpha$.

Variation of area downwash angle with α .- The area downwash angles for the complete model and the model less wing, given in figure 6, are somewhat higher in every case than the values of the corresponding theory. The previously mentioned influence of the vertical tail helps to account for this difference. The agreement in $d\epsilon/d\alpha$ for the complete model and the model less the wing is good throughout except for the complete model at $M = 1.59$ in the negative angle-of-attack range.

In the difference curves of figure 6, the variation of the difference between the downwash values obtained for the complete model and the model-less-wing configuration is compared with the variation of theoretical wing-alone values. This comparison is of uncertain significance because of the unknown magnitude of the interference effects due to the addition of the wing.

The area downwash difference variations at $M = 1.40$ agree very closely with theory while at $M = 1.59$ they indicate a negligible $d\epsilon/d\alpha$ as compared with theory.

Comparison of area downwash angles with force-test results.- The downwash curves from the pressure analysis and the theory are compared with the results of force tests in figure 9. The force-test downwash angles were obtained by determining the tail incidence angle for which the addition of the tail had no effect on the pitching moment.

From the force tests it was also found that the downwash angles corresponding to the vanishing of the pitching-moment increment were essentially the same as those corresponding to the vanishing of the normal-force coefficients. Hence the area downwash from the pressure tests should be an approximation to the force results.

For the complete configuration at both Mach numbers, the pressure data, though indicating slightly lower downwash angles than the force data, show essentially the same values of $d\epsilon/d\alpha$, values which agree reasonably well with theory. Similar agreement between the pressure data and theory is shown for the model-less-wing configuration at $M = 1.40$. No force data are available for the model-less-wing

configuration at $M = 1.40$. For $M = 1.59$ the force and pressure data show dissimilar trends for the model-less-wing configuration, the pressure data showing a considerably higher $d\epsilon/d\alpha$ value. The theoretical value is between both sets of experimental data.

At both Mach numbers, the theoretical results agree that the model-less-wing configuration contributes about the same $d\epsilon/d\alpha$ as the wing alone. The pressure results at $M = 1.40$ credit the model-less-wing configuration with about the same $d\epsilon/d\alpha$ as the wing, but at $M = 1.59$, the pressures indicate that the contribution of the model less wing is considerably more than half of the total $d\epsilon/d\alpha$. The only force-test results at $M = 1.59$ indicate a small body contribution to the total $d\epsilon/d\alpha$.

CONCLUDING REMARKS

From an analysis of pressures measured on the horizontal tail of a supersonic aircraft configuration in the Langley 4- by 4-foot supersonic tunnel at Mach numbers of 1.40 and 1.59, estimates of downwash angle in the plane of the tail are obtained for the complete model and the model less the wing. These results are compared with an approximate application of linearized theory and, where appropriate, with force-test results for the same configuration.

The pressure downwash angles are everywhere greater than those of the theory. This is probably due largely to the neglect of the flow field produced by the vertical tail. For the outboard stations, there is reasonable agreement in the average rate of change of downwash angle with angle of attack.

The pressure and theoretical results indicate that about half the total rate of change of downwash angle with angle of attack is due to the wing at a Mach number of 1.40. At a Mach number of 1.59, theory indicates the same trend. Experimentally, however, pressure downwash angles show a somewhat smaller wing contribution to the rate of change of downwash angle with angle of attack, while on the other hand, force-test results at the same Mach number show a much greater wing contribution.

Langley Aeronautical Laboratory
National Advisory Committee for Aeronautics
Langley Field, Va.

REFERENCES

1. Perkins, Edward W., and Canning, Thomas N.: Investigation of Downwash and Wake Characteristics at a Mach Number of 1.53. I - Rectangular Wing. NACA RM A8L16, 1949.
2. Perkins, Edward W., and Canning, Thomas N.: Investigation of Downwash and Wake Characteristics at a Mach Number of 1.53. II - Triangular Wing. NACA RM A9D20, 1949.
3. Perkins, Edward W., and Canning, Thomas N.: Investigation of Downwash and Wake Characteristics at a Mach Number of 1.53. III - Swept Wings. NACA RM A9K02, 1950.
4. Adamson, D., and Boatright, William B.: Investigation of Downwash, Sidewash, and Mach Number Distribution behind a Rectangular Wing at a Mach Number of 2.41. NACA RM L50G12, 1950.
5. Cummings, J. L., Mirels, H. and Boughman, L. E.: Downwash in the Vortex Region behind a Trapezoidal-Wing Tip at Mach Number 1.91. NACA RM E9H15, 1949.
6. Ellis, Macon C., Jr., and Grigsby, Carl E.: Aerodynamic Investigation at Mach Number 1.92 of a Rectangular Wing and Tail and Body Configuration and Its Components. NACA RM L9L28a, 1950.
7. Spearman, M. Leroy: An Investigation of a Supersonic Aircraft Configuration Having a Tapered Wing with Circular-Arc Sections and 40° Sweepback. Static Longitudinal Stability and Control Characteristics at a Mach Number of 1.40. NACA RM L9L08, 1950.
8. Spearman, M. Leroy, and Hilton, John H., Jr.: An Investigation of a Supersonic Aircraft Configuration Having a Tapered Wing with Circular-Arc Sections and 40° Sweepback. Static Longitudinal Stability and Control Characteristics at a Mach Number of 1.59. NACA RM L50E12, 1950.
9. Lagerstrom, P. A., Graham, Martha E., and Grosslight, G.: Downwash and Sidewash Induced by Three-Dimensional Lifting Wings in Supersonic Flow. Rep. No. SM-13007, Douglas Aircraft Co., Inc., April 14, 1947.
10. Lagerstrom, P. A., and Graham, Martha E.: Methods for Calculating the Flow in the Trefftz-Plane behind Supersonic Wings. Rep. No. SM-13288, Douglas Aircraft Co., Inc., July 28, 1948.

11. Lomax, Harvard, and Sluder, Loma: Downwash in the Vertical and Horizontal Planes of Symmetry behind a Triangular Wing in Supersonic Flow. NACA TN 1803, 1949.
12. Mirels, Harold, and Haefeli, Rudolf C.: Line-Vortex Theory for Calculation of Supersonic Downwash. NACA Rep. 983, 1950. (Formerly NACA TN 1925.)
13. Ferri, Antonio: Application of the Method of Characteristics to Supersonic Rotational Flow. NACA Rep. 841, 1946. (Formerly NACA TN 1135.)
14. Ferri, Antonio: The Method of Characteristics for the Determination of Supersonic Flow over Bodies of Revolution at Small Angles of Attack. NACA TN 1809, 1949.
15. Von Kármán, Theodor, and Moore, Norton B.: Resistance of Slender Bodies Moving with Supersonic Velocities with Special Reference to Projectiles. Trans. A.S.M.E., vol. 54, no. 23, Dec. 15, 1932, pp. 303-310.
16. Tsien, Hsue-Shen: Supersonic Flow over an Inclined Body of Revolution. Jour. Aero. Sci., vol. 5, no. 12, Oct. 1938, pp. 480-483.
17. Cooper, Morton, Smith, Norman F., and Kainer, Julian H.: A Pressure-Distribution Investigation of a Supersonic Aircraft Fuselage and Calibration of the Mach Number 1.59 Nozzle of the Langley 4- by 4-Foot Supersonic Tunnel. NACA RM L9E27a, 1949.
18. Hasel, Lowell E., and Sinclair, Archibald R.: A Pressure-Distribution Investigation of a Supersonic-Aircraft Fuselage and Calibration of the Mach Number 1.40 Nozzle of the Langley 4- by 4-Foot Supersonic Tunnel. NACA RM L50B14a, 1950.
19. Cooper, Morton, and Spearman, M. Leroy: An Investigation of a Supersonic Aircraft Configuration Having a Tapered Wing with Circular-Arc Sections and 40° Sweepback. A Pressure-Distribution Study of the Aerodynamic Characteristics of the Wing at Mach Number 1.59. NACA RM L50C24, 1950.
20. Smith, Norman F., Kainer, Julian H., and Webster, Robert A.: An Investigation of a Supersonic Aircraft Configuration Having a Tapered Wing with Circular-Arc Sections and 40° Sweepback. A Pressure-Distribution Study of the Aerodynamic Characteristics of the Wing at Mach Number 1.40. NACA RM L51C06, 1951.

21. Spreiter, John R., and Sacks, Alvin H.: The Rolling Up of the Trailing Vortex Sheet and Its Effect on the Downwash behind Wings. Jour. Aero. Sci., vol. 18, no. 1, Jan. 1951, pp. 21-32, 72.

TABLE I.- PRESSURE COEFFICIENTS ON HORIZONTAL TAIL FOR MODEL LESS ITS WING

(a) $M = 1.40$

Plane A

α		-5		0		2		4		
$\downarrow t$		2	4	2	4	-2	0	-2	0	2
Upper- surface position, x/c	0.102	0.265	0.200	0.076	-0.002	0.167	0.085	0.089	-0.005	-0.106
	.190	.142	.077	-.037	-.100	.049	-.030	-.024	-.101	-.175
	.279	.064	.007	-.098	-.155	-.017	-.088	-.082	-.158	-.221
	.388	.006	-.042	-.136	-.194	-.061	-.127	-.121	-.194	-.251
	.491	-.038	-.083	-.166	-.221	-.097	-.154	-.150	-.219	-.276
Lower- surface position, x/c	.124	-.205	-.111	.035	.108	-.050	.039	.037	.122	.201
	.221	-.230	-.152	-.031	.041	-.103	-.025	-.028	.050	.127
	.327	-.257	-.188	-.081	-.017	-.149	-.078	-.080	-.012	.058
	.393	-.276	-.211	-.111	-.050	-.174	-.108	-.111	-.048	.018
	.486	-.304	-.252	-.164	-.110	-.221	-.163	-.165	-.108	-.048

Plane B

α		-5		0		2		4		
$\downarrow t$		2	4	2	4	-2	0	-2	0	2
Upper- surface position, x'/c'	0.084	0.237	0.171	0.065	-0.005	0.156	0.075	0.086	0.000	-0.090
	.168	.131	.068	-.034	-.093	.056	-.019	-.008	-.086	-.153
	.260	.058	.003	-.084	-.146	-.006	-.069	-.058	-.133	-.196
	.353	-.007	-.051	-.120	-.172	-.050	-.107	-.097	-.158	-.222
	.442	-.071	-.116	-.169	-.212	-.117	-.166	-.150	-.200	-.248
Lower- surface position, x'/c'	.539	-.078	-.111	-.163	-.191	-.120	-.154	-.149	-.180	-.213
	.786	-.193	-.226	-.262	-.291	-.218	-.257	-.246	-.285	-.309
	.106	-.213	-.122	.005	.075	-.072	.009	.008	.085	.157
	.199	-.233	-.174	-.075	-.011	-.142	-.075	-.077	-.010	.062
	.238	-.241	-.186	-.097	-.036	-.158	-.097	-.099	-.037	.036
	.340	-.285	-.235	-.163	-.105	-.224	-.169	-.172	-.114	-.045
	.428	-.320	-.274	-.221	-.163	-.279	-.221	-.235	-.172	-.112
	.530	-.359	-.320	-.266	-.219	-.323	-.226	-.277	-.226	-.178
	.596	-.377	-.342	-.292	-.243	-.334	-.290	-.299	-.254	-.211
	.733	-.370	-.361	-.323	-.277	-.306	-.323	-.321	-.293	-.255

Plane C

α		-5		0		2		4		
$\downarrow t$		2	4	2	4	-2	0	-2	0	2
Upper- surface position, x/c	0.091	0.183	0.135	0.084	0.030	0.172	0.111	0.136	0.072	0.004
	.185	.080	.027	-.037	-.089	.056	-.005	.020	-.048	-.114
	.288	.042	-.006	-.053	-.100	.018	-.031	-.017	-.073	-.122
	.395	-.020	-.065	-.106	-.143	-.040	-.096	-.069	-.122	-.166
	.492	-.081	-.121	-.160	-.196	-.101	-.146	-.130	-.177	-.210
Lower- surface position, x/c	.122	-.120	-.083	-.020	.045	-.105	-.045	-.066	-.004	.065
	.188	-.183	-.131	-.094	-.028	-.189	-.127	-.161	-.103	-.024
	.288	-.213	-.163	-.139	-.078	-.211	-.150	-.180	-.119	-.053
	.392	-.268	-.221	-.191	-.140	-.251	-.201	-.218	-.172	-.119
	.489	-.317	-.277	-.240	-.194	-.293	-.248	-.262	-.218	-.175

NACA

TABLE I.- PRESSURE COEFFICIENTS ON HORIZONTAL TAIL FOR MODEL LESS ITS WING - Concluded

(b) $M = 1.59$

Plane A

α		-5		-3	-2	0		2	4			6	8			10
i_t		2	4	2	2	2	4	2	-2	0	2	2	-4	-2	2	2
Upper- surface position, x/c	0.102	0.256	0.184	0.203	0.169	0.107	0.026	0.048	0.149	0.047	-0.030	-0.097	0.092	0.033	-0.166	-0.163
	.190	.134	.067	.086	.053	-.010	-.078	-.060	.032	-.063	-.119	-.169	-.018	-.072	-.224	-.119
	.279	.057	-.005	.012	-.017	-.071	-.138	-.119	-.034	-.125	-.174	-.215	-.078	-.127	-.263	-.116
	.388	.002	-.054	-.038	-.064	-.113	-.175	-.158	-.080	-.161	-.210	-.244	-.115	-.163	-.287	-.101
	.491	-.043	-.093	-.077	-.102	-.145	-.204	-.188	-.114	-.189	-.221	-.269	-.148	-.191	-.307	-.068
Lower- surface position, x/c	.124	-.205	-.111	-.116	-.072	.000	.068	.064	-.039	.029	.121	.182	.014	.073	.236	.285
	.221	-.227	-.149	-.157	-.119	-.060	.005	-.061	-.037	.052	.111	-.051	.006	.157	.201	
	.327	-.254	-.185	-.190	-.160	-.107	-.048	-.053	-.139	-.089	-.008	.047	-.100	-.049	.089	.127
	.393	-.271	-.207	-.210	-.186	-.135	-.078	-.086	-.168	-.120	-.044	.006	-.131	-.083	.048	.087
	.486	-.303	-.249	-.252	-.230	-.184	-.131	-.140	-.213	-.174	-.100	-.060	-.185	-.140	-.019	.020

Plane B

α		-5		-3	-2	0		2	4			6	8			10
i_t		2	4	2	2	2	4	2	-2	0	2	2	-4	-2	2	2
Upper- surface position, x/c	0.084	0.230	0.169	0.180	0.151	0.089	0.024	0.039	0.134	0.039	-0.030	-0.089	0.086	0.031	-0.155	-0.205
	.168	.125	.064	.076	.047	-.010	-.070	-.055	.033	-.057	-.111	-.155	-.010	-.061	-.204	-.159
	.260	.051	-.003	.009	-.016	-.065	-.127	-.111	-.026	-.109	-.161	-.199	-.059	-.110	-.237	-.138
	.353	-.011	-.061	-.044	-.066	-.109	-.161	-.146	-.073	-.145	-.194	-.230	-.103	-.141	-.262	-.140
	.442	-.080	-.121	-.110	-.127	-.161	-.207	-.191	-.131	-.200	-.230	-.263	-.158	-.188	-.293	-.146
Lower- surface position, x/c	.539	-.087	-.121	-.111	-.127	-.159	-.188	-.177	-.130	-.183	-.201	-.221	-.159	-.171	-.241	-.105
	.786	-.196	-.232	-.224	-.238	-.263	-.295	-.280	-.235	-.293	-.306	-.312	-.259	-.279	-.318	-.144
	.106	-.216	-.122	-.132	-.091	-.029	.040	.030	-.067	-.005	.080	.133	-.021	.036	.185	.237
	.199	-.238	-.176	-.182	-.155	-.105	-.040	-.055	-.139	-.090	-.011	.041	-.109	-.057	.087	.135
	.238	-.243	-.191	-.196	-.171	-.124	-.061	-.078	-.158	-.114	-.036	.017	-.130	-.079	.056	.102

Plane C

α		-5		-3	-2	0		2	4			6	8			10
i_t		2	4	2	2	2	4	2	-2	0	2	2	-4	-2	2	2
Upper- surface position, x/c	0.091	0.173	0.123	0.137	0.121	0.085	0.031	0.052	0.132	0.056	0.000	-0.039	0.094	0.051	-0.088	-0.118
	.185	.066	.012	.023	.002	-.041	-.095	-.080	.011	-.070	-.122	-.152	-.012	-.054	-.182	-.196
	.288	.027	-.028	-.011	-.027	-.060	-.109	-.096	-.023	-.089	-.131	-.163	-.048	-.085	-.191	-.205
	.395	-.032	-.077	-.069	-.083	-.113	-.156	-.127	-.066	-.152	-.161	-.188	-.109	-.122	-.216	-.226
	.492	-.092	-.133	-.124	-.138	-.164	-.205	-.188	-.128	-.191	-.215	-.235	-.164	-.179	-.259	-.219
Lower- surface position, x/c	.122	-.144	-.115	-.102	-.078	-.044	.012	-.008	-.097	-.054	.027	.052	-.115	-.066	.070	.130
	.188	-.189	-.149	-.168	-.154	-.123	-.059	-.096	-.190	-.144	-.067	-.052	-.202	-.152	-.002	.065
	.288	-.222	-.171	-.205	-.190	-.161	-.109	-.130	-.222	-.182	-.111	-.080	-.197	-.149	-.030	.024
	.392	-.274	-.227	-.257	-.243	-.169	-.183	-.265	-.232	-.232	-.164	-.136	-.224	-.188	-.093	.066
	.489	-.321	-.283	-.301	-.285	-.261	-.213	-.232	-.296	-.274	-.210	-.183	-.260	-.226	-.146	-.116

TABLE II.- PRESSURE COEFFICIENTS ON HORIZONTAL TAIL FOR COMPLETE MODEL

(a) $M = 1.40$

Plane A

	-3					0					2					4					8				
	x/c	-2	0	2	4	-4	-2	0	2	4	-6	-4	-2	0	2	-6	-4	-2	0	2	-6	-4	-2	0	
Upper surface position, x/c	0.102 0.190 0.279 0.368 0.451	0.353 0.239 0.161 0.089 0.063	0.283 0.174 0.097 0.040 0.010	0.280 0.107 0.001 -0.013 -0.053	0.159 0.001 -0.013 -0.073 -0.086	0.321 0.210 0.137 0.070 0.049	0.279 0.150 0.013 -0.032 -0.006	0.186 0.077 0.013 -0.065 -0.060	0.120 0.021 -0.037 -0.074 -0.106	0.046 -0.039 -0.090 -0.153 -0.151	0.327 0.219 0.143 0.092 0.070	0.247 0.134 0.069 0.020 -0.001	0.194 0.083 0.039 -0.019 -0.073	0.118 0.015 -0.043 -0.079 -0.111	0.058 -0.047 -0.098 -0.132 -0.197	0.860 0.147 0.079 -0.027 -0.099	0.184 0.075 0.012 -0.027 -0.099	0.129 0.021 -0.033 -0.070 -0.100	0.059 -0.045 -0.098 -0.131 -0.160	-0.046 -0.112 -0.156 -0.183 -0.207	0.112 0.012 -0.042 -0.094 -0.104	0.031 -0.047 -0.094 -0.127 -0.150	-0.047 -0.111 -0.152 -0.176 -0.197	-0.138 -0.179 -0.213 -0.235 -0.253	
Lower surface position, x/c	0.164 0.221 0.307 0.393 0.466	-0.177 -0.198 -0.222 -0.236 -0.262	-0.103 -0.136 -0.168 -0.186 -0.217	-0.022 -0.066 -0.106 -0.097 -0.163	-0.046 -0.008 -0.057 -0.083 -0.126	-0.103 -0.132 -0.161 -0.182 -0.212	-0.049 -0.090 -0.127 -0.157 -0.185	-0.031 0.043 -0.072 -0.099 -0.140	-0.106 -0.043 -0.008 -0.037 -0.005	-0.164 -0.097 -0.041 -0.008 -0.047	-0.115 -0.142 -0.174 -0.191 -0.223	-0.068 -0.074 -0.081 -0.093 -0.115	-0.035 -0.021 -0.067 -0.091 -0.136	-0.105 0.039 -0.011 0.047 0.012	-0.176 -0.106 -0.119 -0.141 -0.180	-0.017 -0.079 -0.002 -0.119 -0.182	-0.077 -0.002 -0.051 -0.076 -0.125	-0.115 0.050 -0.049 -0.085 -0.063	-0.181 0.109 0.049 0.065 0.005	-0.290 -0.172 -0.105 -0.068 -0.005	-0.119 0.010 -0.007 -0.039 -0.090	-0.210 0.135 0.073 0.112 0.018	-0.279 -0.181 -0.119 -0.072 0.010	-0.386 -0.242 -0.169 -0.113 -0.064	

Plane B

	-3					0					2					4					8				
	x/c	-2	0	2	4	-4	-2	0	2	4	-6	-4	-2	0	2	-6	-4	-2	0	2	-6	-4	-2	0	
Upper surface position, x/c	0.084 0.168 0.260 0.353 0.442 0.539 0.706	0.352 0.225 0.145 0.089 0.042 -0.033 -0.103	0.262 0.157 0.084 0.033 -0.036 -0.074 -0.147	0.199 0.096 0.031 -0.017 -0.070 -0.113 -0.173	0.140 0.041 -0.023 -0.064 -0.110 -0.145 -0.204	0.304 0.198 0.127 0.070 0.021 -0.040 -0.108	0.243 0.137 0.069 0.007 -0.035 -0.096 -0.148	0.173 0.069 0.012 -0.043 -0.080 -0.122 -0.157	0.112 0.018 -0.037 -0.093 -0.128 -0.165 -0.207	0.043 -0.037 -0.093 -0.128 -0.165 -0.197 -0.237	0.312 0.207 0.133 0.065 0.000 -0.059 -0.105	0.234 0.129 0.064 0.016 -0.002 -0.079 -0.111	0.183 0.080 0.018 -0.002 -0.079 -0.123 -0.175	0.112 0.016 -0.043 -0.079 -0.121 -0.167 -0.215	0.186 0.042 -0.097 -0.130 -0.169 -0.201 -0.237	0.246 0.144 0.077 0.009 -0.024 -0.072 -0.136	0.177 0.076 0.017 -0.068 -0.102 -0.140 -0.172	0.126 0.030 -0.068 -0.102 -0.150 -0.186 -0.219	0.042 -0.037 -0.090 -0.143 -0.178 -0.205 -0.234	-0.041 -0.099 -0.143 -0.182 -0.208 -0.229 -0.259	0.114 0.083 -0.063 -0.081 -0.103 -0.136 -0.169	0.041 -0.030 -0.081 -0.105 -0.135 -0.161 -0.207	-0.016 -0.090 -0.128 -0.157 -0.183 -0.199 -0.236	-0.122 -0.162 -0.186 -0.203 -0.230 -0.253 -0.266	
Lower surface position, x/c	0.106 0.199 0.292 0.340 0.428 0.530 0.596 0.733	-0.182 -0.215 -0.222 -0.254 -0.289 -0.319 -0.303 -0.284	-0.115 -0.157 -0.165 -0.207 -0.232 -0.262 -0.296	-0.036 -0.092 -0.105 -0.160 -0.211 -0.224 -0.243 -0.270	0.024 -0.046 -0.062 -0.121 -0.177 -0.224 -0.243 -0.270	-0.116 -0.158 -0.169 -0.212 -0.256 -0.272 -0.276	-0.068 -0.121 -0.134 -0.184 -0.235 -0.257 -0.267	-0.007 -0.067 -0.083 -0.092 -0.103 -0.120 -0.132 -0.144	-0.080 -0.002 -0.021 -0.092 -0.154 -0.209 -0.240 -0.251	-0.134 -0.049 -0.064 -0.073 -0.089 -0.109 -0.126 -0.124	-0.188 -0.171 -0.163 -0.186 -0.202 -0.221 -0.236 -0.267	-0.050 -0.064 -0.062 -0.086 -0.106 -0.128 -0.146 -0.166	-0.010 -0.054 -0.029 -0.010 -0.079 -0.103 -0.123	-0.076 0.009 -0.029 -0.055 -0.086 -0.113 -0.134 -0.165	-0.141 -0.050 -0.119 -0.135 -0.172 -0.196 -0.210 -0.250	-0.056 -0.119 -0.051 -0.085 -0.139 -0.196 -0.222 -0.255	-0.028 -0.051 -0.002 -0.065 -0.098 -0.161 -0.204 -0.262	-0.097 -0.002 -0.068 -0.088 -0.131 -0.193 -0.244 -0.262	-0.144 0.050 0.065 0.008 -0.114 -0.176 -0.204 -0.236	-0.208 0.108 0.079 0.001 -0.114 -0.180 -0.262 -0.296	-0.067 0.073 0.046 0.062 -0.009 -0.111 -0.162 -0.236	-0.174 0.073 0.046 0.082 -0.009 -0.104 -0.175 -0.260	-0.218 0.117 0.082 0.103 -0.001 -0.084 -0.145 -0.176	-0.264 -0.175 -0.128 -0.091 -0.013 -0.064 -0.128 -0.191	

Plane C

	-3					0					2					4					8				
	x/c	-2	0	2	4	-4	-2	0	2	4	-6	-4	-2	0	2	-6	-4	-2	0	2	-6	-4	-2	0	
Upper surface position, x/c	0.091 0.189 0.288 0.395 0.492	0.263 0.146 0.080 0.057 0.014	0.204 0.088 0.040 0.044 0.028	0.147 0.031 -0.000 -0.044 -0.092	0.097 -0.021 -0.042 -0.080 -0.129	0.267 0.151 0.094 0.047 -0.063	0.214 0.095 0.036 0.001 -0.082	0.154 0.036 -0.043 -0.060 -0.099	0.095 -0.018 -0.088 -0.120 -0.119	0.040 -0.068 -0.090 -0.120 -0.160	0.293 0.173 0.083 0.071 -0.001	0.223 0.106 0.061 0.029 -0.000	0.180 0.062 0.029 -0.027 -0.083	0.121 0.008 -0.074 -0.089 -0.123	0.053 -0.028 0.135 0.036 -0.039	0.292 0.135 0.076 -0.022 -0.073	0.226 0.117 0.035 -0.026 -0.019	0.177 0.076 0.025 -0.022 -0.019	0.149 0.025 -0.006 -0.049 -0.144	0.083 -0.029 0.006 -0.102 -0.144	0.012 -0.045 0.063 -0.133 -0.181	0.167 0.033 -0.074 -0.082 -0.105	0.135 0.033 -0.052 -0.072 -0.105	0.080 -0.024 -0.097 -0.124 -0.148	0.019 -0.080 -0.102 -0.136 -0.178
Lower surface position, x/c	0.122 0.188 0.288 0.392 0.499	-0.140 -0.187 -0.219 -0.262 -0.291	-0.082 -0.139 -0.179 -0.224 -0.259	-0.033 -0.089 -0.130 -0.186	-0.005 -0.059 -0.086 -0.126	-0.130 -0.174 -0.203 -0.244	-0.089 -0.143 -0.185 -0.225	-0.019 -0.099 -0.137 -0.179	-0.047 -0.037 -0.034 -0.077	-0.092 -0.011 -0.037 -0.144	-0.191 -0.226 -0.238 -0.261	-0.114 -0.160 -0.115 -0.167	-0.051 -0.073 -0.073 -0.119	-0.018 -0.015 -0.066 -0.112	-0.087 -0.023 -0.065 -0.121 -0.151	-0.160 -0.131 -0.085 -0.226	-0.075 -0.131 -0.085 -0.171	-0.007 -0.043 -0.100	-0.052 0.005 -0.040	-0.127 -0.011 -0.040	-0.049 -0.007 -0.133	-0.049 -0.079 -0.107	-0.102 -0.033 -0.113 -0.185	-0.102 -0.013 -0.069	

NACA

TABLE II.- PRESSURE COEFFICIENTS ON HORIZONTAL TAIL FOR COMPLETE MODEL - Concluded

(b) $\kappa = 1.59$

Plane A	α		-5		-3		-2		0				2		4				6		8				10	
	ξ		4		0		4		0		4		0		4		0		4		0		4		0	
	$\frac{x}{c}$		$\frac{x}{c}$		$\frac{x}{c}$		$\frac{x}{c}$		$\frac{x}{c}$		$\frac{x}{c}$		$\frac{x}{c}$		$\frac{x}{c}$		$\frac{x}{c}$		$\frac{x}{c}$		$\frac{x}{c}$		$\frac{x}{c}$		$\frac{x}{c}$	
Upper-surface position, $\frac{x}{c}$	0.102	0.230	0.303	0.238	0.174	0.205	0.330	0.280	0.214	0.149	0.079	0.231	0.303	0.231	0.179	0.107	0.025	0.258	0.210	0.125	0.076	0.163	0.091	0.006	0.006	0.006
	0.190	0.109	0.183	0.180	0.077	0.090	0.122	0.161	0.096	0.038	0.080	0.112	0.183	0.112	0.062	0.003	0.060	0.142	0.093	0.014	0.020	0.091	0.006	0.006	0.006	0.006
	0.279	0.043	0.108	0.092	-0.004	0.026	0.136	0.091	0.035	-0.019	-0.072	0.048	0.113	0.047	0.000	-0.055	-0.110	0.072	0.089	-0.044	-0.074	0.006	0.006	0.006	0.006	0.006
	0.368	-0.004	0.057	0.005	-0.050	-0.080	0.065	0.041	-0.010	-0.062	-0.109	0.004	0.063	0.002	-0.042	-0.094	-0.146	0.027	-0.014	-0.064	-0.111	-0.063	0.006	0.006	0.006	0.006
	0.451	-0.037	0.019	-0.027	-0.079	-0.050	0.043	0.005	-0.044	-0.091	-0.136	-0.088	0.024	-0.031	-0.071	-0.123	-0.169	-0.008	-0.046	-0.113	-0.137	-0.071	0.006	0.006	0.006	0.006
Lower-surface position, $\frac{x}{c}$	0.124	-0.050	-0.123	-0.047	-0.018	-0.007	-0.151	-0.097	0.000	0.058	0.120	-0.088	-0.114	-0.019	0.036	-0.118	-0.180	-0.048	0.008	0.066	0.150	0.062	0.006	0.006	0.006	0.006
	0.221	-0.054	-0.148	-0.087	-0.034	-0.077	-0.177	-0.131	-0.065	0.002	0.058	-0.073	-0.143	-0.064	-0.018	0.049	-0.113	-0.089	-0.044	0.020	0.079	0.062	0.006	0.006	0.006	0.006
	0.327	-0.133	-0.181	-0.186	-0.079	-0.099	-0.204	-0.163	-0.105	-0.045	0.005	-0.112	-0.175	-0.107	-0.065	-0.034	0.053	-0.128	-0.091	-0.036	0.020	0.062	0.006	0.006	0.006	0.006
	0.431	-0.154	-0.199	-0.147	-0.103	-0.121	-0.220	-0.185	-0.128	-0.071	-0.025	-0.132	-0.193	-0.131	-0.091	-0.041	0.018	-0.149	-0.115	-0.063	0.010	0.060	0.006	0.006	0.006	0.006
	0.486	-0.190	-0.225	-0.183	-0.142	-0.159	-0.249	-0.215	-0.166	-0.115	-0.074	-0.169	-0.225	-0.170	-0.118	-0.084	-0.039	-0.186	-0.156	-0.113	-0.063	0.006	0.006	0.006	0.006	0.006

Plane B	α		-5		-3		-2		0				2		4				6	
---------	----------	--	----	--	----	--	----	--	---	--	--	--	---	--	---	--	--	--	---	--

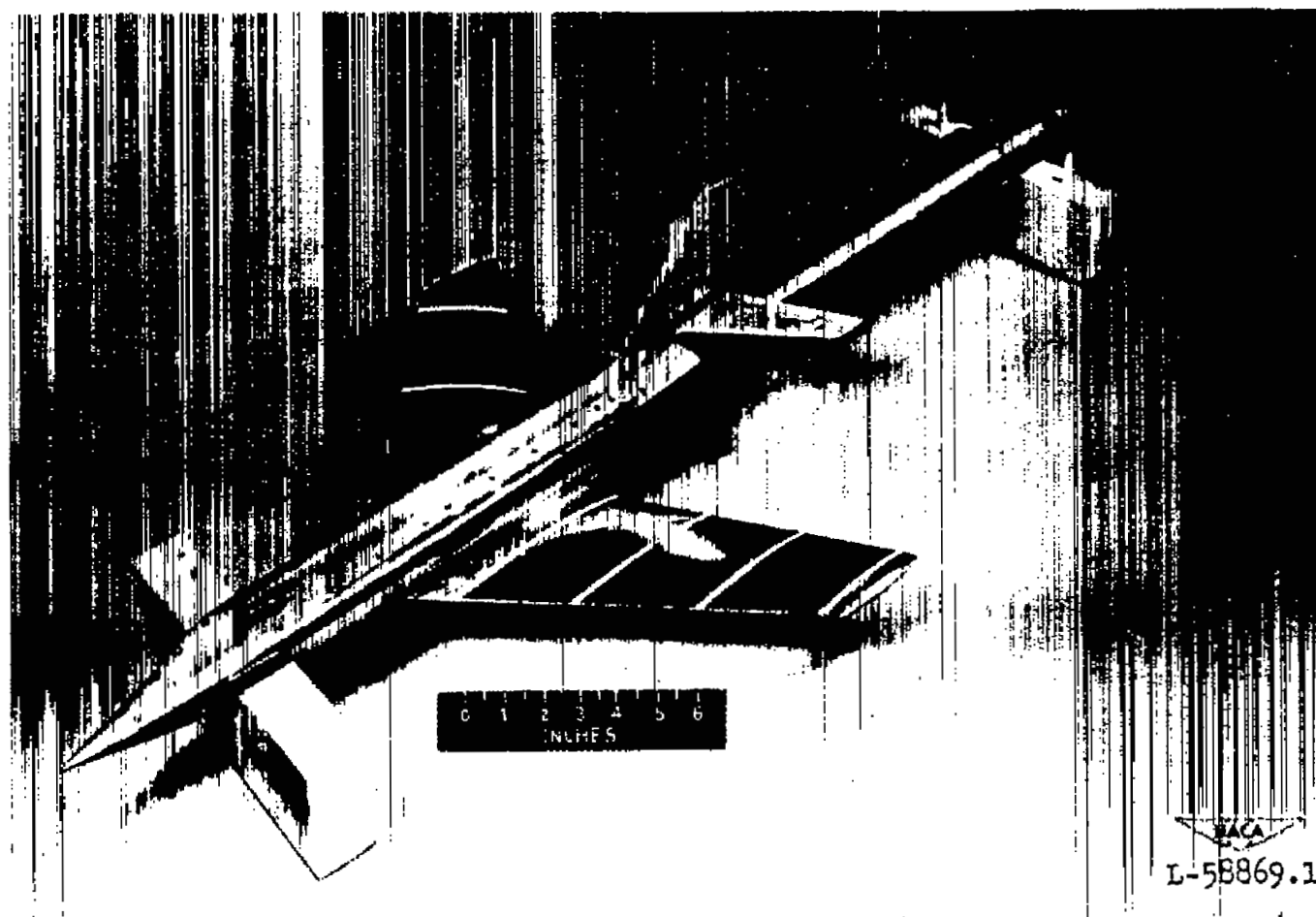


Figure 1.- Pressure model of supersonic aircraft configuration tested in the Langley 4- by 4-foot supersonic tunnel.

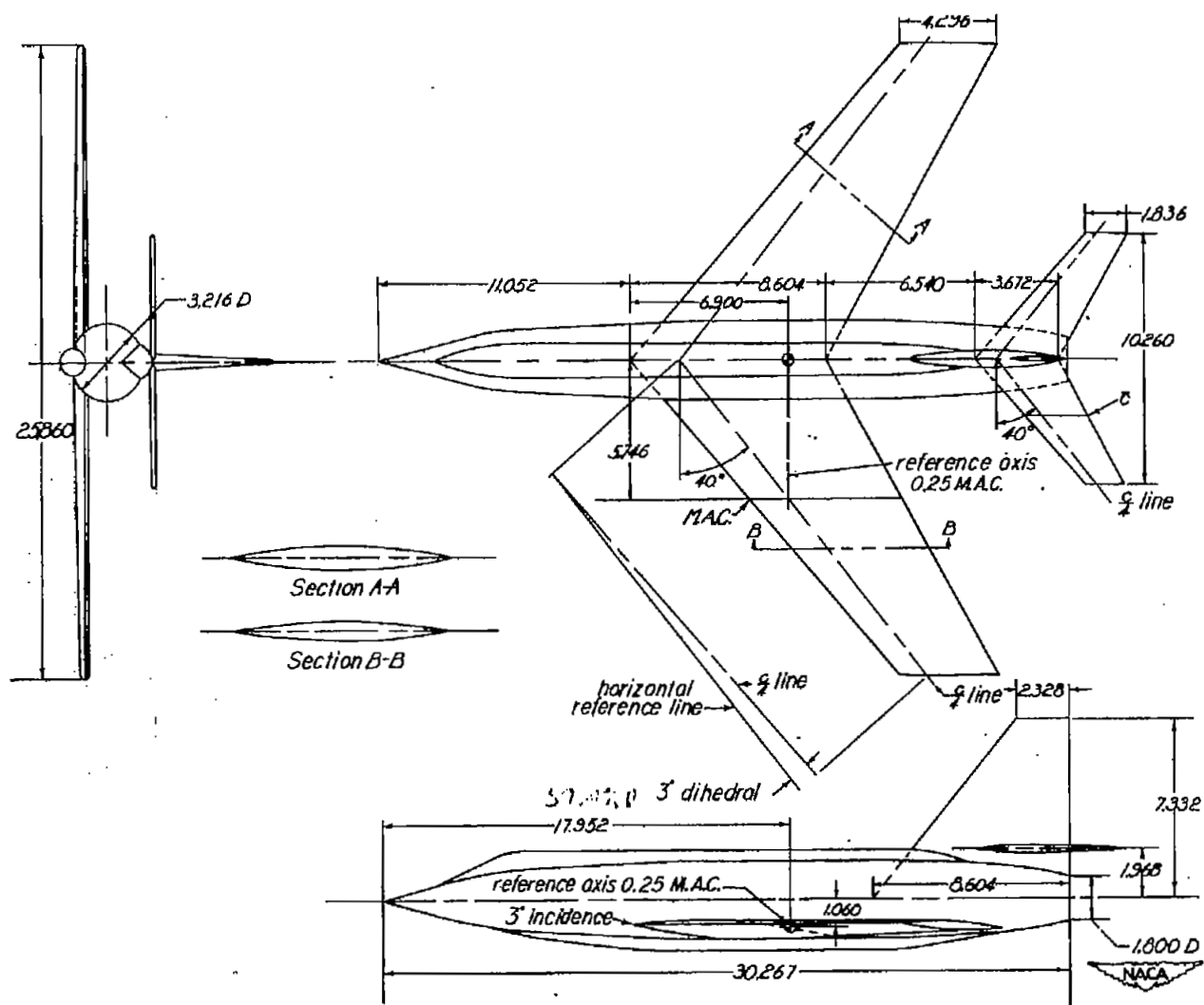


Figure 2.- Details of model of supersonic aircraft configuration. Dimensions in inches unless otherwise noted.



Figure 3.- Installation of pressure model of supersonic aircraft configuration tested in the Langley 4- by 4-foot supersonic tunnel.

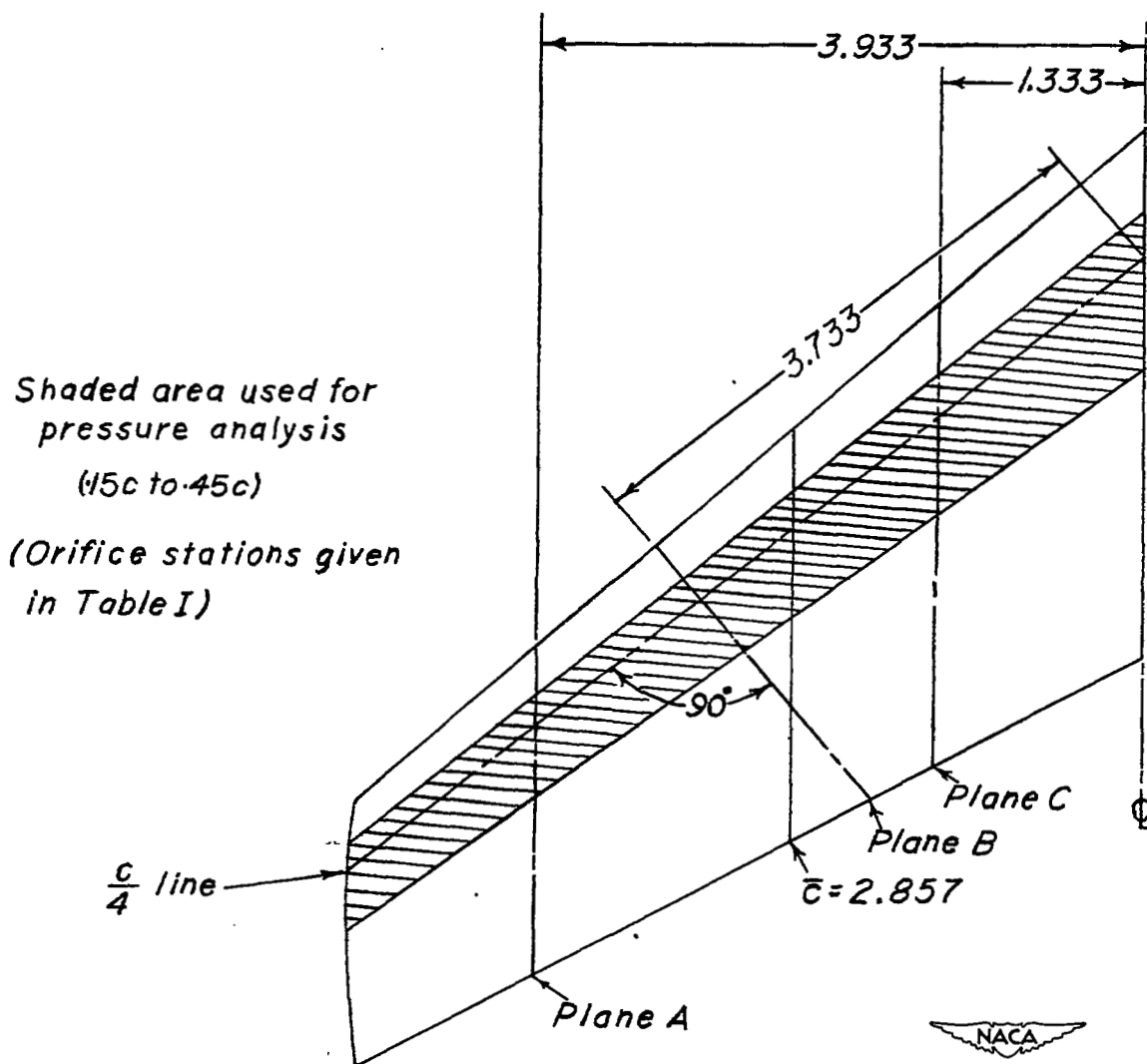


Figure 4.- Schematic diagram of horizontal tail. Dimensions in inches unless otherwise noted.

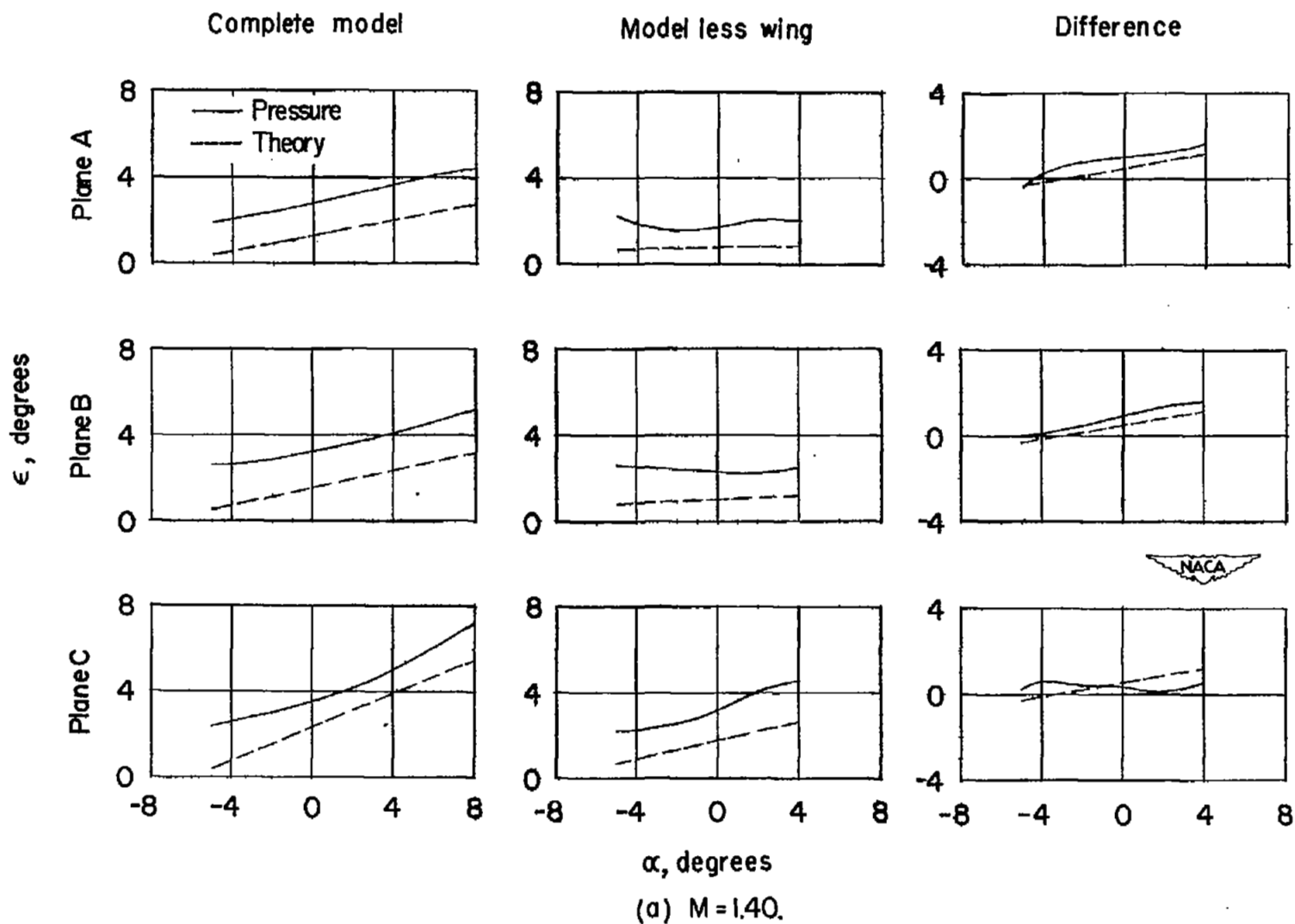


Figure 5.- Variation with angle of attack of point downwash angle on the 15-percent constant chord line.

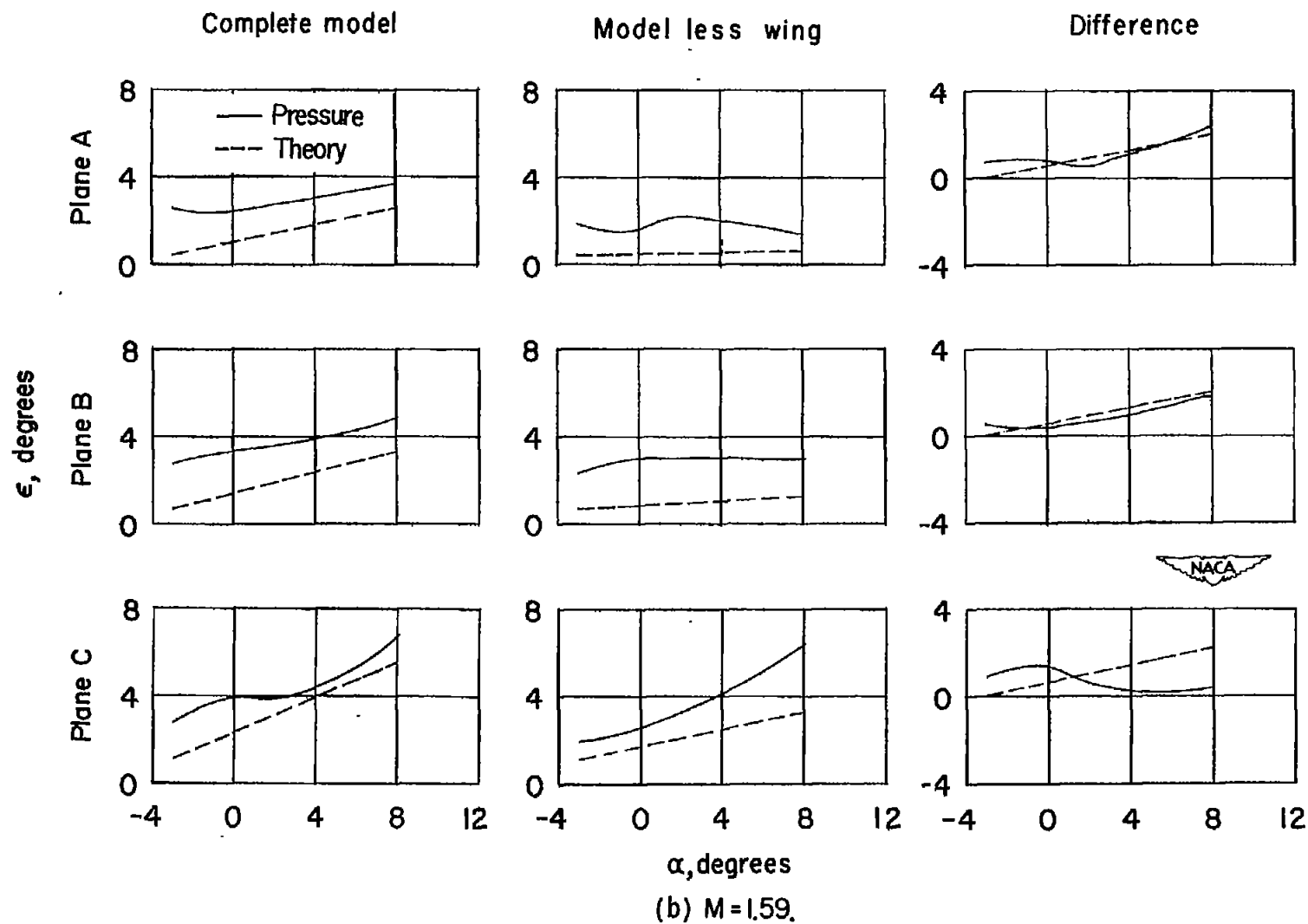


Figure 5.- Concluded.

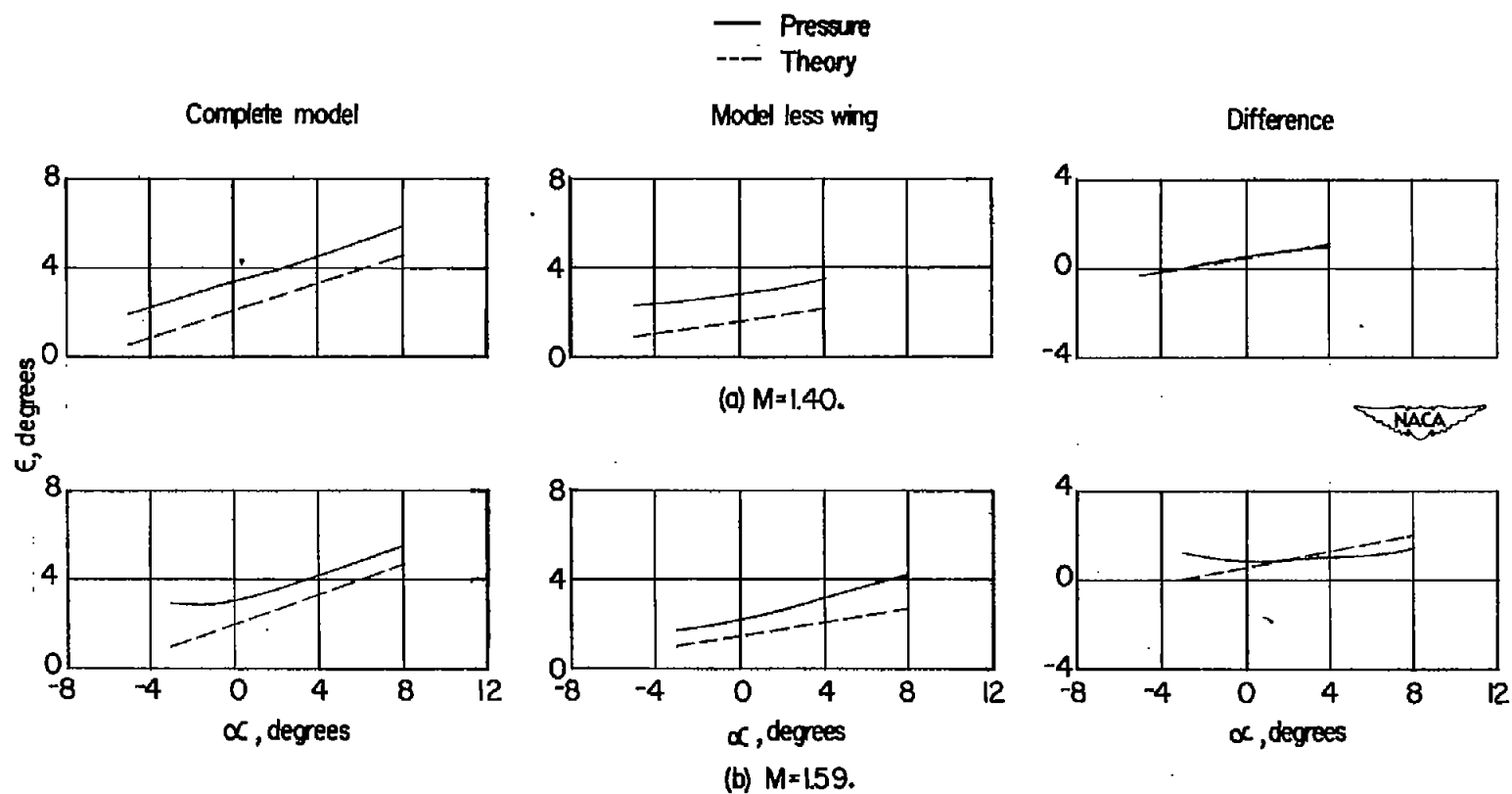


Figure 6.- Variation with angle of attack of area downwash angle.

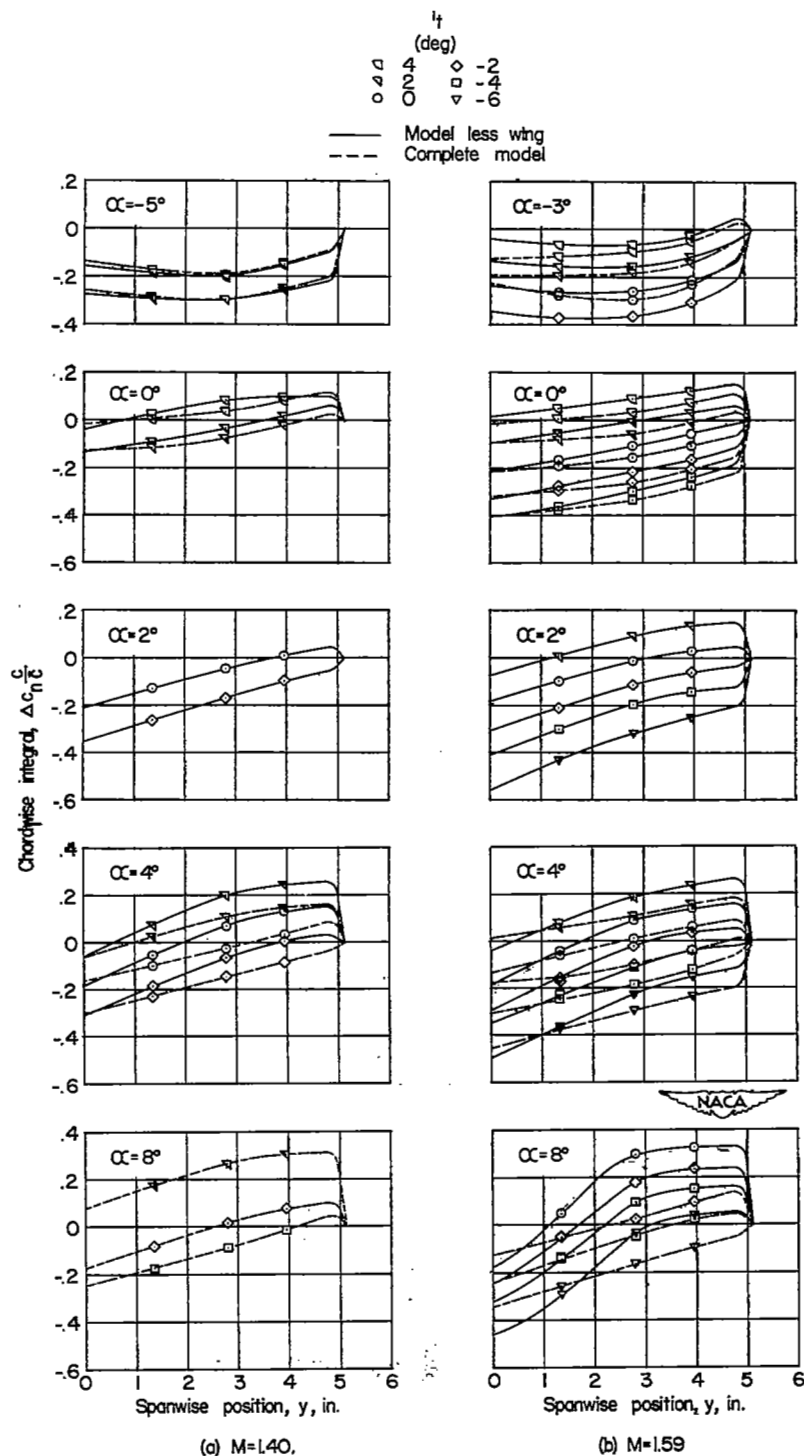
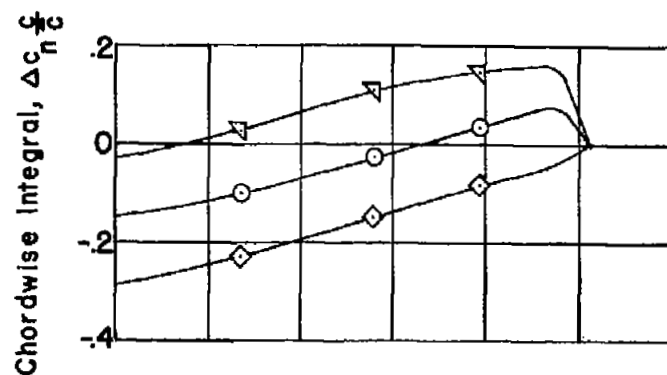
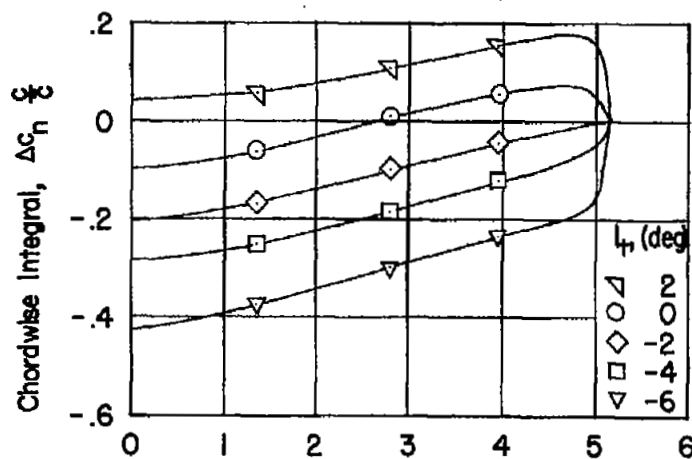
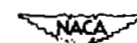
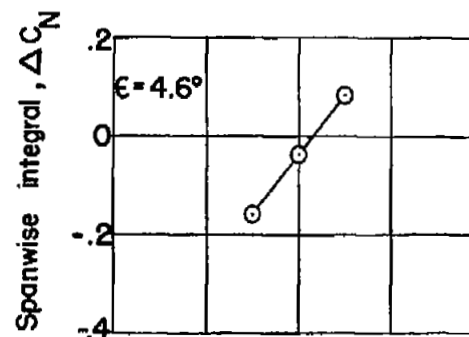


Figure 7.- Span-loading curves for the strip between the 15- and 45-percent constant chord lines on the horizontal tail.



(a) M=1.40.



(b) M=1.59.

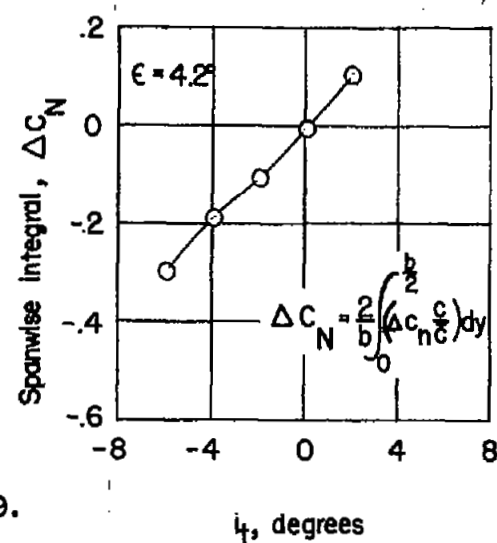


Figure 8.- Sample evaluation of an area downwash angle for the complete model at $\alpha = 4^\circ$.

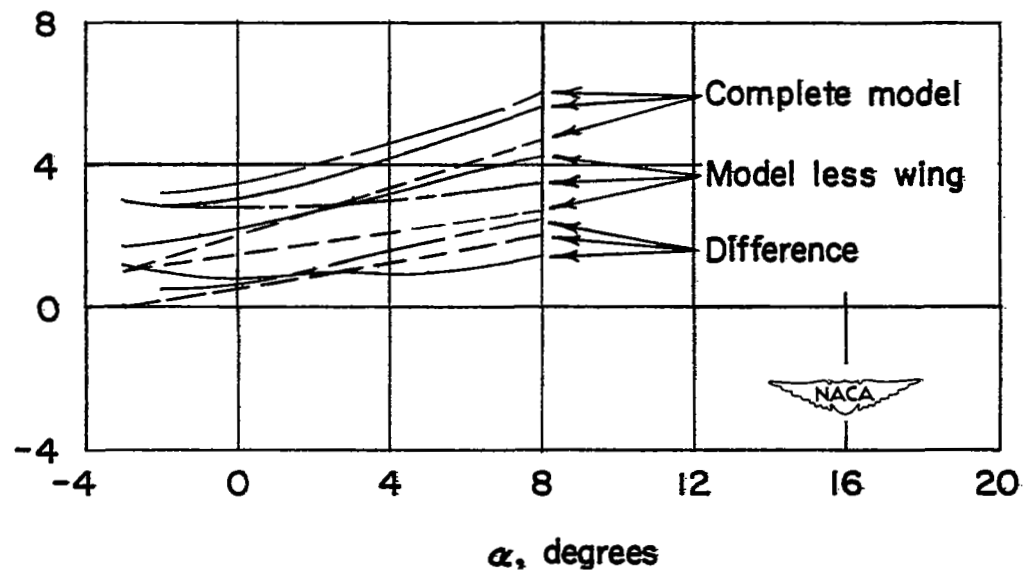
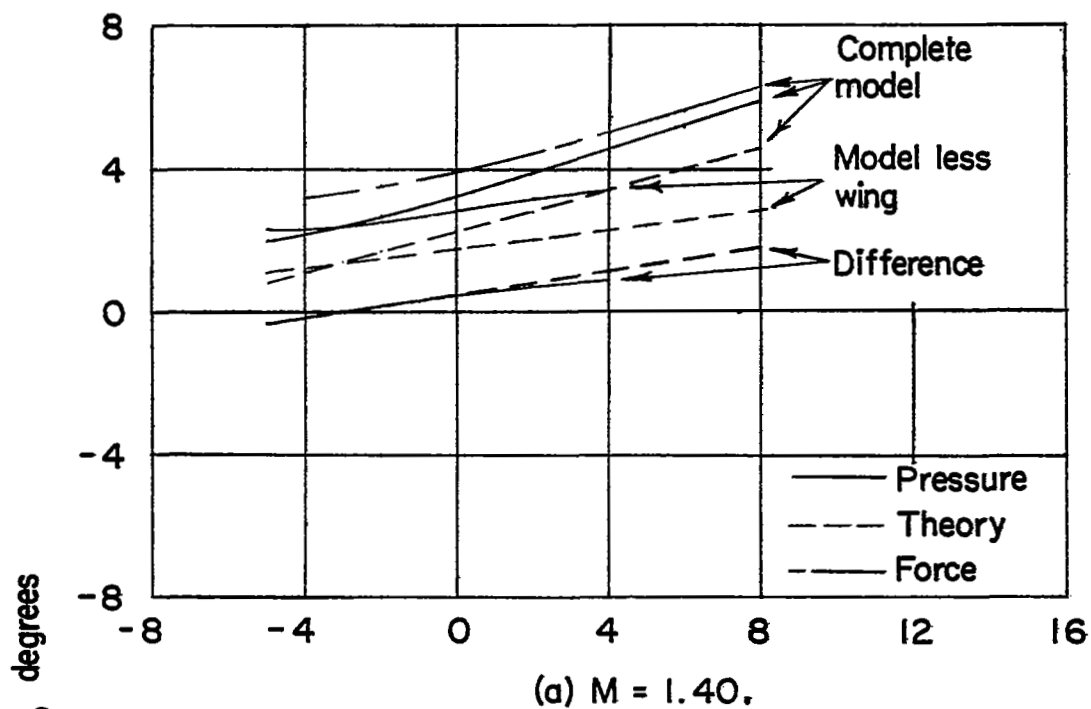


Figure 9.- Comparison of variation of downwash angle with angle of attack for various analyses.

SECURITY INFORMATION

NASA Technical Library



3 1176 01436 9129

[REDACTED]